

# General properties of phase diagrams of heavy-fermion metals

V. R. SHAGINYAN<sup>1,2</sup> (a), A. Z. MSEZANE<sup>2</sup>, K. G. POPOV<sup>3</sup>, G. S. JAPARIDZE<sup>2</sup> and V. A. KHODEL<sup>4,5</sup>

<sup>1</sup> Petersburg Nuclear Physics Institute, Gatchina, 188300, Russia

<sup>2</sup> Clark Atlanta University, Atlanta, GA 30314, USA

<sup>3</sup> Komi Science Center, Ural Division, RAS, Syktyvkar, 167982, Russia

<sup>4</sup> Russian Research Center Kurchatov Institute, Moscow, 123182, Russia

<sup>5</sup> McDonnell Center for the Space Sciences & Department of Physics, Washington University, St. Louis, MO 63130, USA

PACS 71.10.Hf – Non-Fermi-liquid ground states; electron phase diagrams

PACS 64.70.Tg – Quantum phase transitions

PACS 71.27.+a – Strongly correlated electron systems; heavy fermions

**Abstract.** - We study the temperature-magnetic field  $T-B$  phase diagrams of heavy fermion (HF) metals, and show that at sufficiently high temperatures outside the ordered phase the crossover temperature  $T^*(B)$ , regarded as the energy scale, follows a linear  $B$ -dependence, crossing the origin of the  $T-B$  phase diagram. This behavior of  $T^*(B)$  constitutes the general property, and is formed by the presence of fermion condensation quantum phase transition hidden within the ordered phase. Our result is in good agreement with the experimental  $T-B$  phase diagram of the HF metals  $\text{YbRh}_2\text{Si}_2$ ,  $\text{Yb}(\text{Rh}_{0.93}\text{Co}_{0.07})_2\text{Si}_2$ , and  $\text{Yb}(\text{Rh}_{0.94}\text{Ir}_{0.06})_2\text{Si}_2$ . To support our observations, we analyze the isothermal magnetization  $M$ , and demonstrate that  $dM/dT$  exhibits a universal temperature behavior over magnetic field scaling. The obtained results are in good agreement with the corresponding data collected on  $\text{YbRh}_2\text{Si}_2$  as a function of magnetic field at different temperatures under hydrostatic pressure.

**Introduction.** – Quantum criticality occupies the low temperature area of the  $T-B$  phase diagram of the heavy-fermion (HF) metals. In this area HF metals exhibit a specific behavior known as non-Fermi liquid (NFL) behavior, which is induced by a phase transition at zero temperature, driven by pressure, doping or magnetic field. While approaching the quantum critical point (QCP), related to the phase transition, the effective mass  $M^*$  grows continuously, causing strong deviations from Landau's Fermi liquid (LFL) theory. In the  $T-B$  phase diagram, such NFL states are separated from those of LFL by the crossover temperature  $T^*(B)$ , given by the behavior of  $M^*$  and regarded as the energy scale, which vanishes at the QCP [1]. The QCP can be related to different quantum phase transitions such as antiferromagnetic (AF) phase transition, e.g.  $\text{YbRh}_2\text{Si}_2$  [2], ferromagnetic (FM) one, e.g.  $\text{CePd}_{1-x}\text{Rh}_x$  [3], superconducting (SC), e.g.  $\text{CeCoIn}_5$  [4], or even the QCP can be located at the origin of the  $T-B$  phase diagram with the paramagnetic (PM) ground state, e.g.  $\text{CeRu}_2\text{Si}_2$  [5]. Nonetheless, such

a diverse transitions do not violate the universal scaling behavior of the thermodynamic properties, and they are indicative of the diversity generated by a single phase transition represented by the fermion condensation quantum phase transition (FCQPT) [1]. It is reasonable to expect that fingerprints of that phase transition emerge at sufficiently high temperatures  $T_d^* > T_{NL}$ , where  $T_{NL}$  is the critical temperature of the AF phase transition which is taken as an example.

Recent study poses a challenging problem for the condensed matter physics, revealing that the  $T-B$  phase diagrams of HF metals  $\text{CeCoIn}_5$  [4],  $\text{YbRh}_2\text{Si}_2$ ,  $\text{Yb}(\text{Rh}_{0.93}\text{Co}_{0.07})_2\text{Si}_2$ , and  $\text{Yb}(\text{Rh}_{0.94}\text{Ir}_{0.06})_2\text{Si}_2$ , and the evolution of the  $T-B$  diagram of  $\text{YbRh}_2\text{Si}_2$  under the application of hydrostatic pressure  $P$  indicates a hidden QCP at zero field, while  $T^*(B)$  follows a linear  $B$ -dependence at sufficiently high fields or temperatures outside the ordered phase [2, 4]. It has been observed that at sufficiently high temperatures  $T$  outside the AF phase the crossover temperature  $T^*(B)$  follows almost a linear  $B$ -dependence, crossing the origin of the  $T-B$  phase diagram [2]. Phase diagrams for  $\text{Yb}(\text{Rh}_{0.93}\text{Co}_{0.07})_2\text{Si}_2$  and

(a)Email: vrshag@thd.pnpi.spb.ru

$\text{Yb}(\text{Rh}_{0.94}\text{Ir}_{0.06})_2\text{Si}_2$  can be obtained from the phase diagram for  $\text{YbRh}_2\text{Si}_2$  by applying positive/negative pressure. The negative chemical pressure is caused by Ir substitution and the positive by Co substitution. This can be confirmed by performing hydrostatic pressure experiments on clean undoped  $\text{YbRh}_2\text{Si}_2$  and comparing the results with ambient pressure ones on  $\text{Yb}(\text{Rh}_{1-x}\text{Co}_x)_2\text{Si}_2$ , demonstrating that the Co and Ir-induced disorder can not be the reason for the modifications of the corresponding  $T - B$  phase diagram [2,6]. Thus, the phase diagrams obtained in measurements on  $\text{Yb}(\text{Rh}_{0.93}\text{Co}_{0.07})_2\text{Si}_2$  and  $\text{Yb}(\text{Rh}_{0.94}\text{Ir}_{0.06})_2\text{Si}_2$  can be viewed as a general experimental  $T - B$  phase diagram of  $\text{YbRh}_2\text{Si}_2$  that allows one to reveal QCP hidden in the AF phase.

In this letter, to resolve the challenging problem mentioned above, we study the  $T - B$  phase diagrams of HF metals, and show that at sufficiently high temperatures outside the ordered phase the crossover temperature  $T^*(B)$  follows a linear  $B$ -dependence, and crosses the origin of the  $T - B$  phase diagram. Upon analyzing the experimental global  $T - B$  phase diagram of  $\text{YbRh}_2\text{Si}_2$ , we show that FCQPT represents QCP hidden in the AF phase. Our analysis agrees well with the experimental  $T - B$  phase diagrams of the HF metals  $\text{YbRh}_2\text{Si}_2$ ,  $\text{Yb}(\text{Rh}_{0.93}\text{Co}_{0.07})_2\text{Si}_2$ , and  $\text{Yb}(\text{Rh}_{0.94}\text{Ir}_{0.06})_2\text{Si}_2$ . We calculate the isothermal magnetization  $M$ , and demonstrate that  $dM/dT$  exhibits a universal temperature over magnetic field scaling. Our results are in good agreement with data collected on  $\text{YbRh}_2\text{Si}_2$ , and support our conclusion on the nature of the hidden QCP.

### Energy scales and phase diagrams of HF metals.

– At  $T = 0$ , a quantum phase transition is driven by a nonthermal control parameter such as number density  $x$ , magnetic field  $B$  or pressure  $P$ . At the QCP, situated at  $x = x_{FC}$  and related to FCQPT, the effective mass  $M^*$  diverges. We note that there are different types of instabilities of normal Fermi liquids related to perturbations of the initial quasiparticle spectrum  $\varepsilon(p)$  and occupation numbers  $n(p)$ , associated with the emergence of a multi-connected Fermi surface, see e.g. [1,7]. Depending on the parameters and analytical properties of the Landau interaction, such instabilities lead to several possible types of restructuring of the initial Fermi liquid ground state. In fact, at elevated temperatures the systems located at these transition points, exhibit the behavior typical to those located at FCQPT [1]. Therefore, we do not consider the specific properties of systems located at different topological transitions, but rather focus on the behavior of the system located near FCQPT. Beyond the FCQPT, the system shapes FC that leads to the formation of a topologically protected flat band [8,9]. We note that microscopic analysis confirms that the formation is robust when tuning interaction, temperature, and chemical potential [10], and these results are in accordance with [8,9].

For the reader convenience, and to present a coherent analysis of the  $T^*(B)$  behavior based on the recent exper-

imental facts [2,6], we start with consideration of the auxiliary phase diagrams reported in figs. 1, 2, 3, and 4 which were partly considered in Refs. [1,11]. The schematic  $T - x$  phase diagram of the system driven to the FC state by varying the number density  $x$  is presented in fig. 1. Upon approaching the critical density  $x_{FC}$  the system remains in the LFL region at sufficiently low temperatures, as shown by the shadowed area. The temperature range of this area shrinks as the system approaches QCP, and  $M^*(x \rightarrow x_{FC})$  diverges. At this QCP shown by the arrow in fig. 1, the system demonstrates the NFL behavior down to the lowest temperatures. Beyond the critical point the behavior remains NFL even at  $T \rightarrow 0$ . It is determined by the temperature-independent residual entropy  $S_0$  [1,12]. In that case at  $T \rightarrow 0$ , the system approaches a quantum critical line (QCL) (shown by the vertical arrow and the dashed line in fig. 1) rather than a QCP. Upon reaching the QCL from above at  $T \rightarrow 0$  the system undergoes the first order quantum phase transition, making the residual entropy  $S_0$  vanish. As seen from fig. 1, at rising temperatures the system located before QCP does not undergo a phase transition, and transits from the NFL to the LFL regime. At finite temperatures there is no boundary (or phase transition) between the states of the system located before or behind QCP, shown by the arrows. Therefore, at elevated temperatures the properties of systems with  $x/x_{FC} < 1$  or with  $x/x_{FC} > 1$  become indistinguishable.

As seen from fig. 1, the location of the system is controlled by the number density  $x$ . At  $x/x_{FC} > 1$ , the system is located before FCQPT, and demonstrates the LFL behavior at low temperatures. We speculate that such a state can be induced by applying positive pressure, including positive chemical pressure, as occurs for the case of  $\text{Yb}(\text{Rh}_{0.93}\text{Co}_{0.07})_2\text{Si}_2$ . HF metals, such as  $\text{CeRu}_2\text{Si}_2$  are placed at FCQPT, as shown in fig. 1 by the dash arrow. Such metals exhibit PM ground state and NFL behavior to the lowest temperatures. On the other hand, by diminishing  $x$ ,  $x/x_{FC} < 1$ , the system is shifted beyond FCQPT, and is at the quantum critical line depicted by the dashed line. In that case the system demonstrates the NFL behavior at any finite temperatures. We assume that such a state can be induced by the application of negative pressure, including negative chemical pressure, as is the case for  $\text{Yb}(\text{Rh}_{0.94}\text{Ir}_{0.06})_2\text{Si}_2$ . At low temperatures and above the critical line, the system has the finite entropy  $S_0$  and its NFL state is strongly degenerate. The degeneracy stimulates the emergence of different phase transitions, lifting degeneracy and removing the entropy  $S_0$ . The NFL state can be captured by other states such as SC (like SC state in  $\text{CeCoIn}_5$ ), or AF (like the AF state in  $\text{YbRh}_2\text{Si}_2$ ) [1,12]. The diversity of phase transitions at low temperatures is one of the most spectacular features of the physics of many HF metals and strongly correlated compounds. Within the scenario of ordinary quantum phase transitions, it is hard to understand why these transitions are so different from each other and their critical temperatures are so extremely small. However, such diversity is

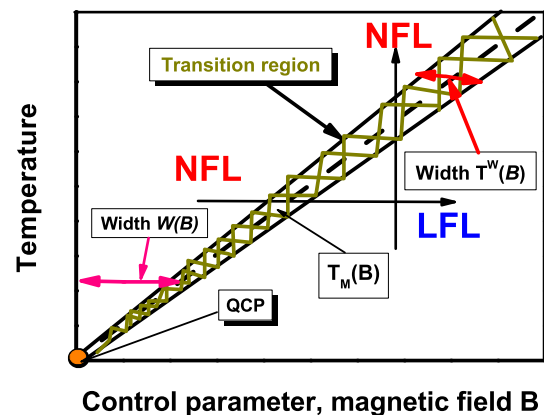
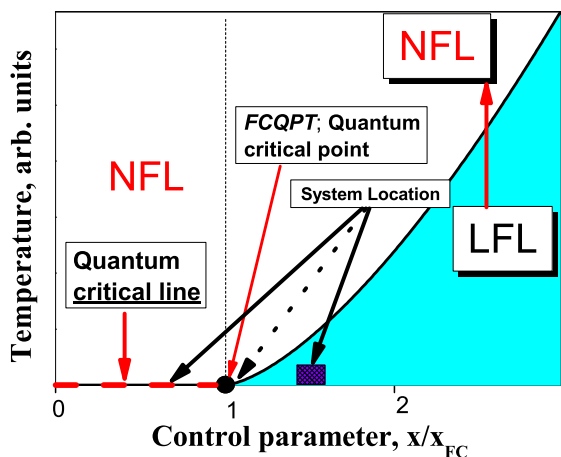


Fig. 1: (Color online) Schematic  $T-x$  phase diagram of system with FC. The number density  $x$  is taken as the control parameter and depicted as  $x/x_{FC}$ . At  $x/x_{FC} > 1$  and at sufficiently low temperatures, the system is in the LFL state as shown by the shadowed area. This location of the system is depicted by both the solid square and the arrow. The vertical arrow illustrates the system moving in the LFL-NFL direction along  $T$  at fixed control parameter. At  $x/x_{FC} < 1$  the system is shifted beyond the QCP, and is at the quantum critical line depicted by the dashed line and shown by the vertical arrow. At any finite low temperatures  $T > 0$  the system possesses finite entropy  $S_0$  and exhibits the NFL behavior.

Fig. 2: (Color online) Schematic  $T-B$  phase diagram of HF liquid with magnetic field as the control parameter. The vertical and horizontal arrows show LFL-NFL and NFL-LFL transitions at fixed  $B$  and  $T$ , respectively. At  $B = 0$  the system is in its NFL state, having a flat band, and demonstrates NFL behavior down to  $T \rightarrow 0$ . The hatched area separates the NFL phase and the weakly polarized LFL phase and represents the transition region. The dashed line in the hatched area represents the function  $T_M(B) \simeq T_{FC}^*$  given by  $T_M \simeq a_1 \mu_B B$ . The functions  $W(B) \propto T$  and  $T^W(B) \propto T$  shown by two-headed arrows define the width of the NFL state and the transition area, respectively. The QCP located at the origin and indicated by the arrow denotes the critical point at which the effective mass  $M^*$  diverges and both  $W(B)$  and  $T^W(B)$  tend to zero.

endemic to systems with a FC, since the FC state should be altered as  $T \rightarrow 0$  so that the excess entropy  $S_0$  is shed before zero temperature is reached. At finite temperatures this takes place by means of some phase transitions which can compete, shedding the excess entropy [1, 7].

The schematic  $T-B$  phase diagram of a HF liquid is presented in fig. 2, with the magnetic field  $B$  serving as control parameter. The NFL regime reigns at elevated temperatures and fixed magnetic field. With  $B$  increasing, the system is driven from the NFL region to the LFL domain. The magnetic-field-tuned QCP is indicated by the arrow and located at the origin of the phase diagram, since application of any magnetic field destroys the flat band and shifts the system into the LFL state [1, 5, 13]. Near the magnetic-field-tuned QCP, a deeper insight into the behavior of  $M^*(B, T)$  can be achieved using some "internal" (or natural) scales. Namely,  $M^*(B, T)$  reaches its maximum value  $M_{max}^*$  at some temperature  $T_M \simeq a_1 \mu_B B$ , where  $a_1$  is a dimensionless factor and  $\mu_B$  is the Bohr magneton, see e.g. [1]. It is convenient to introduce the internal scales  $M_{max}^*$  and  $T_M$  to measure the effective mass and temperature. Thus, we divide the effective mass  $M^*$  and the temperature  $T$  by the values,  $M_{max}^*$  and  $T_M$ , respectively. This generates the normalized effective mass  $M_N^* = M^*/M_{max}^*$  and the normalized temperature  $T_N = T/T_M$ .  $M_N^*(T_N)$  can be well approximated by a simple universal interpolating function [1]. The interpolation

is valid between the LFL and NFL regimes and represents the universal scaling behavior of  $M_N^*$

$$M_N^*(y) \approx c_0 \frac{1 + c_1 y^2}{1 + c_2 y^{8/3}}. \quad (1)$$

Here,  $y = T_N = T/T_M$ ,  $c_0 = (1 + c_2)/(1 + c_1)$ ,  $c_1, c_2$  are fitting parameters. Thus, in the presence of magnetic field eq. (1) describes the scaling behavior of the effective mass as a function of  $T$  versus  $B$  - the curves  $M_N^*$  at different magnetic fields  $B$  merge into a single one in terms of the normalized variable  $y = T/T_M$ . Since the variables  $T$  and  $B$  enter symmetrically, eq. (1) describes the scaling behavior of  $M_N^*(B, T)$  as a function of  $B$  versus  $T$ . In fig. 2, the hatched area denoting the transition region separates the NFL state from the weakly polarized LFL state and contains the dashed line tracing the transition region,  $T_M(B) \simeq T_{FC}^*$ . Referring to eq. (1), this line is defined by the function  $T_{FC}^* \propto \mu_B B$ , and the width  $W(B)$  of the NFL state is seen to be proportional to  $T$ . Similarly, it can be shown that the vertical width  $T^W(B)$  of the transition region is also proportional to  $T$ .

We now construct the  $T-B$  schematic phase diagram of a HF metal like  $\text{YbRh}_2\text{Si}_2$  shown in fig. 3. The inset in fig. 3 demonstrates the scaling of the normalized effective mass  $M_N^*$  versus the normalized temperature  $T_N$ . The

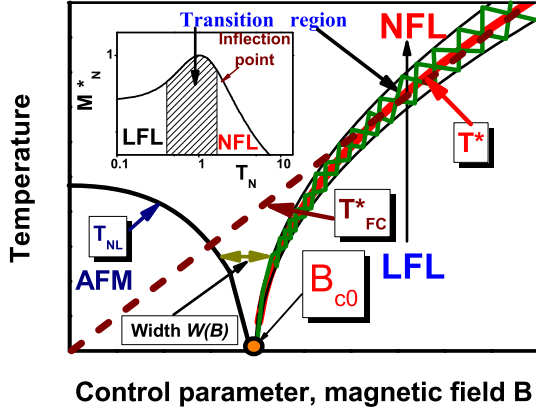


Fig. 3: (Color online) Schematic  $T - B$  phase diagram of a HF metal with magnetic field as control parameter. The AF phase boundary line is shown by the arrow and plotted by the solid curve, representing the Néel temperature  $T_{NL}$ . The hatched area separates the NFL phase and the weakly polarized LFL one and represents the transition region. The solid curve inside the hatched area represents the transition temperature  $T^*$ . The dashed line  $T_{FC}^*(B) \propto B\mu_B$  shows the transition temperature provided that the AF state were absent. The function  $W(B) \propto T$  shown by the two-headed arrow defines the total width of both the NFL state and the transition area. The inset shows a schematic plot of the normalized effective mass versus the normalized temperature. The transition region, where  $M_N^*$  reaches its maximum at  $T_N = T/T_M = 1$ , is shown as the hatched area in both the main panel and the inset. Arrows indicate the transition region and the inflection point  $T_{inf}$  in the  $M_N^*$  plot.

LFL phase prevails at  $T \ll T_M$ , followed by the  $T^{-2/3}$  regime at  $T \gtrsim T_M$ . The latter phase is designated as NFL due to the strong temperature dependence of the effective mass in it. The region  $T \simeq T_M$  encompasses the transition between the LFL regime with almost constant effective mass and the NFL behavior. When constructing the phase diagram in fig. 3, we assumed that the AF order prevails, destroying the  $S_0$  term at low temperatures. At  $B = B_{c0}$ , the HF liquid acquires a flat band, where  $B_{c0}$  is a critical magnetic field, such that at  $T \rightarrow 0$  the application of magnetic field  $B \gtrsim B_{c0}$  destroys the AF state restoring the PM one with LFL behavior. In some cases  $B_{c0} = 0$  as in the HF metal  $\text{CeRu}_2\text{Si}_2$  (see e.g. [5]), while in  $\text{YbRh}_2\text{Si}_2$ ,  $B_{c0} \simeq 0.06$  T [13]. Obviously,  $B_{c0}$  is defined by the specific system properties; therefore we consider it as a parameter. At elevated temperature and fixed magnetic field the NFL regime is dominant. With  $B$  increasing, the system is driven from the NFL to the LFL domain. The magnetic-field-tuned QCP is indicated by the arrow and is located at  $B = B_{c0}$ . The hatched area denotes the transition region, and separates the NFL state from the weakly polarized LFL one. This area contains both the dashed line tracing  $T_{FC}^*(B)$  and the solid curve  $T^*(B)$ . Referring to eq. (1), the latter is defined by

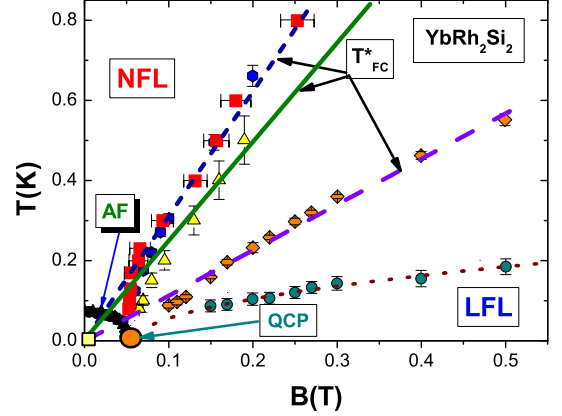


Fig. 4: (Color online)  $T - B$  phase diagram for  $\text{YbRh}_2\text{Si}_2$ . Solid circles represent the boundary between AF and NFL states. The solid circles along the dotted curve denote the boundary of the NFL and LFL regions [13, 14]. The solid square at the origin represents FCQPT. The dotted curve represents the function  $\sqrt{B - B_{c0}}$  [1]. The solid line represents  $T_{FC}^* \propto B\mu_B$ , and shows the linear fit to  $T^*(B)$ . The emphasis is placed on the relatively high temperatures, therefore, the lines  $T_{FC}^*$  deviate from the experimental points at decreasing temperatures. Diamonds marking  $T^*$  along the dash line signify the maxima  $T_M$  of  $C/T$  [15]. The transition temperature  $T^*$ , determined from magnetostriction (solid squares and the short dash line), longitudinal magnetoresistivity (triangles and the solid line), and susceptibility (solid circles and the short dash line) [14] is also reported.

the function  $T^* \propto \mu_B B$  and merges with  $T_{FC}^*(B)$  at relatively high temperatures, and  $T^* \propto \mu_B(B - B_{c0})$  at lower  $T \sim T_{NL}$ , with  $T_{NL}(B)$  being the Néel temperature. As seen from eq. (1), both the width  $W(B)$  of the NFL state and the width of the transition region are proportional to  $T$ . The AF phase boundary line is shown by the arrow and depicted by the solid curve. As mentioned above, the dashed line  $T_{FC}^*(B) \propto B\mu_B$  represents the transition temperature provided that the AF state were absent. In that case the FC state is destroyed by any weak magnetic field  $B \rightarrow 0$  at  $T \rightarrow 0$  and the dashed line  $T_{FC}^*$  crosses the origin, as is displayed in fig. 3. At  $T \gtrsim T_{NL}(B = 0)$  the transition temperature  $T_{FC}^*(B)$  coincides with  $T^*(B)$  shown by the solid curve, since the properties of the system are given by its local free energy, describing the PM state of the system. One might say that the system "does not remember" the AF state, emerging at lower temperatures. This observation is in good agreement with the data collected on the HF metal  $\text{YbRh}_2\text{Si}_2$ .

**The HF metal  $\text{YbRh}_2\text{Si}_2$  under chemical and hydrostatic pressure.** – The above findings are summarized in the phase diagram of fig. 4. At relatively high temperatures  $T \gtrsim T_{NF}(B = 0)$  the transition temperature  $T^*$ , obtained in measurements on  $\text{YbRh}_2\text{Si}_2$  [13–15],

is well approximated by the straight lines representing  $T_{FC}^*$ . It is seen that the straight lines deviate from the experimental points at relatively low temperatures. Also from fig. 4, the slope of the dash line (representing the maxima of the specific heat  $C/T$ ) is different from that of the short dash line (representing maxima of the susceptibility  $\chi(T)$ ). Such behavior is determined by the fact that the maxima of  $C/T$  and  $\chi(T)$  are defined from the two different relations, determining the inflection points of the entropy:

$$\frac{\partial^2 S}{\partial T^2} = 0, \quad \frac{\partial^2 S}{\partial B^2} = 0, \quad (2)$$

respectively. The theory of FC shows that the inflection points exist under the condition that the system is located near FCQPT [1].

Panels A, B, C of fig. 5 are focused on the behavior of the transition temperature  $T^*(B)$  extracted from measurements of kinks in  $\hat{M}(B) = \mathbf{M} + B(d\mathbf{M}/dB)$  [2], where  $\mathbf{M}$  is the magnetization. Positions of the kinks are represented by diamonds in fig. 5. It is seen from the panel A of fig. 5, that at  $T \gtrsim T_{NL}(B=0)$ , the transition temperature  $T^*$  of  $\text{YbRh}_2\text{Si}_2$  is well approximated by the line  $T_{FC}^*$ .  $T_d \sim B_{c0}$  is the temperature at which the line  $T_{FC}^*$  starts to deviate from the experimental data. Indeed, it is seen from fig. 2 that the width  $W \sim T^W \sim T \sim B$ . Approaching QCP at  $B \sim B_{c0}$ , as seen from fig. 3, the width narrows,  $W \sim (B - B_{c0})$ , and  $T_{FC}^*$  deviates from  $T^*$ . As mentioned above, upon using nonthermal tuning parameters like the number density  $x$ , the NFL regime may disappear and the LFL is restored. In our simple model, applying positive pressure  $P$  leads to the increase of the density  $x$  which in turn leads to transition from FCQPT to the LFL state. Figure 1 shows that the above actions move the electronic system of  $\text{YbRh}_2\text{Si}_2$  into the shaded area characterized by the LFL behavior at low temperatures. The new location of the system, represented by  $\text{Yb}(\text{Rh}_{0.93}\text{Co}_{0.07})_2\text{Si}_2$ , is shown by the arrow pointing at the solid square. We note that the positive chemical pressure in the considered case is induced by Co substitution [2, 6]. As a result, the application of magnetic field  $B \simeq B_{c0}$  does not drive the system to its FCQPT with the divergent effective mass because the QCP has already been destroyed by the positive pressure, as shown in panel B of fig. 5. Here  $B_{c0}$  is the critical magnetic field that eliminates the corresponding AF order. At  $B < B_{c0}$  and diminishing temperatures, the system enters the AF state with the LFL behavior. As a result, the effective mass given by eq. (1) becomes  $T$ -independent and the width  $W(B)$  remains constant inside the AF phase. At  $B > B_{c0}$  and increasing temperature, the system, moving along the vertical arrow, transits from the LFL regime to the NFL one. At relatively high temperatures both  $\text{YbRh}_2\text{Si}_2$  and  $\text{Yb}(\text{Rh}_{0.93}\text{Co}_{0.07})_2\text{Si}_2$  are in their PM states. As a result,  $T^*$  is well approximated by the straight line  $T_{FC}^*$ . This behavior coincides with the experimental data [2, 6] reported on panels A, B of fig. 5. The system located above QCL

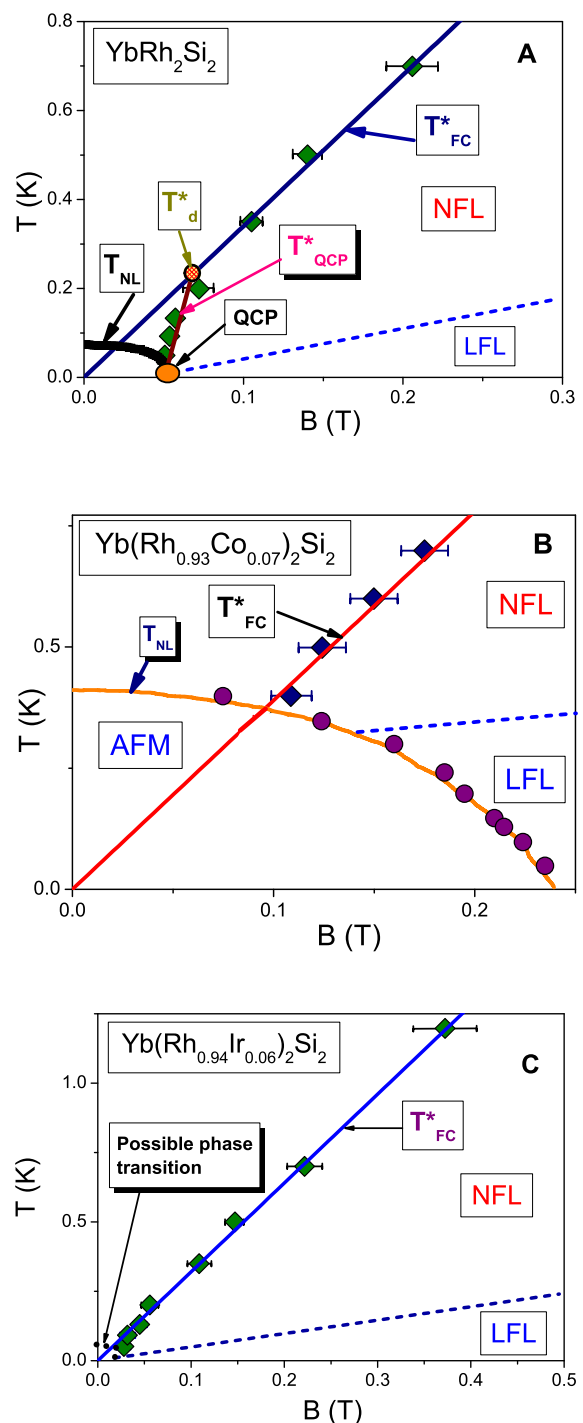


Fig. 5: (Color online)  $T - B$  phase diagrams for the three HF metals:  $\text{YbRh}_2\text{Si}_2$  (A);  $\text{Yb}(\text{Rh}_{0.93}\text{Co}_{0.07})_2\text{Si}_2$  (B);  $\text{Yb}(\text{Rh}_{0.94}\text{Ir}_{0.06})_2\text{Si}_2$  (C). In panels A and B, the AF phase boundaries [2] are shown by the solid lines. The diamonds correspond to the measurements of  $T^*(B)$  extracted from the analysis of the  $\hat{M}(B)$  function [2].  $T_d$  is the temperature at which the line  $T_{FC}^*$  starts to deviate from the experimental data. In panel C, the phase boundary of possible phase transition is shown by dotted curve. The solid straight lines depict the transition temperature  $T_{FC}^*(B)$ . The short dash lines represent schematically the boundary between NFL and LFL regions.

exhibits the NFL behavior down to the lowest temperatures unless it is captured by a phase transition. The behavior exhibited by the system located above QCL agrees with the experimental observations of the QCP evolution in  $\text{YbRh}_2\text{Si}_2$  under the application of negative chemical pressure induced by Ir substitution [2, 6]. To explain the latter behavior, we propose a simple model that the application of negative pressure reduces  $x$  so that the electronic system of  $\text{YbRh}_2\text{Si}_2$  moves from QCP to a new position over QCL shown by the dash arrow in fig. 1. Thus, the electronic system of  $\text{Yb}(\text{Rh}_{0.94}\text{Ir}_{0.06})_2\text{Si}_2$  is located at QCL and possesses a flat band, while the entropy includes  $S_0$ . We predict that at temperature decreasing, the electronic system of  $\text{Yb}(\text{Rh}_{0.94}\text{Ir}_{0.06})_2\text{Si}_2$  is captured by a phase transition, since the NFL state above QCL is strongly degenerate and the term  $S_0$  has to vanish. As temperature decreases, this degeneracy is lifted by some phase transition which can be possibly detected through the LFL state accompanying it. The tentative boundary line of that transition is shown by the short dashed line in fig. 5, panel C. It is also seen from panel C of fig. 5, that at elevated temperatures  $T^*$  is well approximated by the function  $T_{FC}^*$ . Thus, at relatively high temperatures the curve  $T_{FC}^*(B)$ , shown in panels A, B, C of fig. 5 by the solid lines, coincides with  $T^*(B)$  depicted by the diamonds. The preceding discussion demonstrates that the local properties of the system are given by its local free energy. This local free energy defines the NFL behavior which is formed by the presence of FCQPT, as it is reported in fig. 1.

To confirm the above consideration of the phase diagrams, we describe both low temperature magnetization measurements carried out under pressure  $P$  and the  $T-B$  phase diagram of  $\text{YbRh}_2\text{Si}_2$  near its magnetic-field-tuned QCP [6, 16]. To carry out a quantitative analysis of the scaling behavior of  $-\Delta M^*(B, T)/\Delta T$ , we calculate the entropy  $S(B, T)$  and employ the well-known thermodynamic equality  $dM/dT = dS/dB \simeq \Delta M/\Delta T$  [1, 6, 16]. Figure 6, panel a, reports the normalized  $(dS/dB)_N$  as a function of the normalized magnetic field. The function  $(dS/dB)_N$  is obtained by normalizing  $(dS/dB)$  by its maximum taking place at  $B_M$ , and the field  $B$  is scaled by  $B_M$ . It is seen from fig. 6, panel a, that our calculations are in good agreement with the experimental data and the fitting functions  $-(\Delta M/\Delta T)_N$  show the scaling behavior over three decades in the normalized magnetic field. fig. 6, panel b, presents the temperature  $T_M$ , at which the maximum  $-(\Delta M/\Delta T)$  takes place, as a function of magnetic field  $B$ . At  $T_M \simeq T_d$  the line  $T_{FC}^*$  starts to deviate from the experimental data, where  $T_d$  is shown in fig. 5, panel A.

**Summary and acknowledgements.** — We have carried out a comprehensive theoretical study of the  $T-B$  phase diagrams of HF metals such as  $\text{YbRh}_2\text{Si}_2$  and considered the evolution of these diagrams under the application of negative/positive pressure. We have observed that at sufficiently high temperatures outside the AF

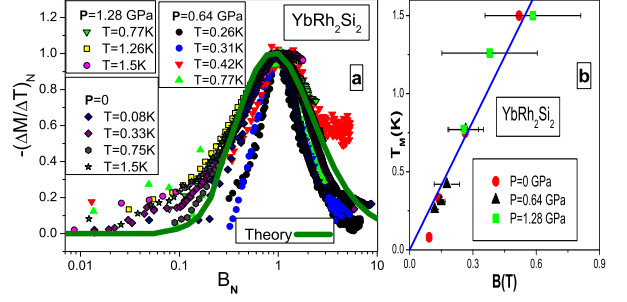


Fig. 6: (Color online) Panel a: The normalized magnetization difference divided by temperature increment  $-(\Delta M/\Delta T)_N$  vs normalized magnetic field at fixed temperature and pressure (listed in the legend in the upper left corner) is extracted from the data collected on  $\text{YbRh}_2\text{Si}_2$  [6, 16]. Panel b:  $T_M$  versus  $B$  is obtained under the application of hydrostatic pressure depicted in the legend and extracted from the measurements [6, 16]. The solid line shows the linear fit to  $T^*(B)$ , and represents  $T_{FC}^*$ .

phase the transition temperature  $T^*(B)$  follows a linear  $B$ -dependence, and collapses on the universal line  $T_{FC}^*(B)$  through the origin. This behavior is in agreement with experimental facts, signifies the general properties of the phase diagram, and is induced by the presence of FCQPT hidden within the AF phase.

This work was partly supported by the RFBR # 14-02-00044, U.S. DOE, Division of Chemical Sciences, Office of Energy Research and AFOSR.

## REFERENCES

- [1] SHAGINYAN V. R., AMUSIA M. YA., MSEZANE A. Z. and POPOV K. G., *Phys. Rep.*, **492** (2010) 31.
- [2] BRANDO M. *et al.*, *Phys. Status Solidi B*, **459** (2013) 285.
- [3] SERENI J. G. *et al.*, *Phys. Rev. B*, **75** (2007) 024432.
- [4] TOKIWA Y., BAUER E. D. AND P. GEGENWART, *Phys. Rev. Lett.*, **111** (2013) 107003.
- [5] TAKAHASHI D. *et al.*, *Phys. Rev. B*, **67** (2003) 180407(R).
- [6] TOKIWA Y. *et al.*, *J. Phys. Soc. Jpn.*, **78** (2009) 123708.
- [7] KHODEL V. A., CLARK J. W. and ZVEREV M. V., *Phys. Rev. B*, **78** (2008) 075120.
- [8] VOLOVIK G. E., *JETP Lett.*, **53** (1991) 222.
- [9] VOLOVIK G. E., *JETP Lett.*, **59** (1994) 830.
- [10] YUDIN D. *et al.*, *Phys. Rev. Lett.*, **112** (2014) 070403.
- [11] SHAGINYAN V. R. *et al.*, *JETP Lett.*, **96** (2012) 397.
- [12] KHODEL V. A., ZVEREV M. V. and YAKOVENKO V. M., *Phys. Rev. Lett.*, **95** (2005) 236402.
- [13] GEGENWART P. *et al.*, *Phys. Rev. Lett.*, **89** (2002) 056402.
- [14] GEGENWART P. *et al.*, *Science*, **315** (2007) 969.
- [15] OESCHLER N. *et al.*, *Physica B*, **403** (2008) 1254.
- [16] TOKIWA Y. *et al.*, *Phys. Rev. Lett.*, **102** (2009) 066401.